Available online at www.sciencedirect.com
ScienceDirect
Mathematics and Computers in Simulation 167 (2020) 308–324
MATHEMATICS AND COMPUTERS IN SIMULATION
www.elsevier.com/locate/matcom

Original articles

Direct torque control improvement of a variable speed DFIG based on a fuzzy inference system

W. Ayrir[a,*], M. Ourahou[a], B. El Hassouni[a], A. Haddi[b]

[a] *Laboratory of Innovative Technologies (LTI), University of ABDELMALEK ESSAÄDI, (ENSA) Tangier, Morocco*
[b] *Advanced Sciences and Technologies team, University of ABDELMALEK ESSAÄDI, (ENSATe) Tetouan, Morocco*

Received 29 August 2017; received in revised form 10 May 2018; accepted 16 May 2018
Available online 30 May 2018

Abstract

In this paper, a fuzzy direct torque control (DTC) for a variable speed doubly fed induction generator (DFIG) based wind turbine is investigated. The DTC has been widely applied to doubly fed induction machines in recent years due to the high performances that it provides in comparison with the classical field oriented control. Meanwhile, it has a major drawback that is the significant torque and flux undulations generated by the hysteresis band controllers. To overcome this problem, the improvement of this technique by removing these controllers is proposed in this paper. The proposed control technique is based on replacing the hysteresis controllers by a fuzzy inference system which will have the same inputs as these controllers plus the sector angle determination so that the look-up table can be replaced by a fuzzy rule-base matrix. The simulation was performed in MATLAB/SIMULINK, and the results obtained make it possible to evaluate the performance of the proposed technique over the classical one.

Keywords: MPPT; DFIG; Direct torque control; Fuzzy logic

1. Introduction

Wind energy represents a significant promising source of renewable energy. It has undoubtedly been the most growing source in terms of installed capacity [27]. According to a report published by the Global Wind Energy Council (GWEC) in 25 April 2017 [13], the cumulative wind energy installed capacity reached 486.8 GW in the end of 2016, and it is expected to reach 800 GW by 2021. Despite this growth, its share in the total world electricity production remains limited, about 4% at the end of 2016 [23], but it is expected to reach 8% by 2018, 12% by 2020 and 20% by 2030 [27,4,16].

* Corresponding author.
E-mail address: ayrir-ouiam@hotmail.com (W. Ayrir).

https://doi.org/10.1016/j.matcom.2018.05.014

Meanwhile, in wind power industry, the concept of a variable-speed wind turbine has been receiving increasing attention because it is more controllable, efficient and has good power quality. Therefore, the choice of the best generator and power converters options is crucial. Currently and over the last few years, the use of DFIG in wind generation systems has received an increasing attention due to many advantages that they present over other types of generators, such as the variable-speed operation with reduced mechanical stress [25], the reactive power compensation due to the converters that are sized to transit only a fraction of the nominal power (about 25% to 30%) and the reduced power losses in the converters [12,9,18].

To control the DFIG, researchers have proposed many different control techniques in the literature. The direct torque control has been and still is one of the most used ones. It is a robust control strategy that has been proposed and applied in mid-1980s for induction machine drives. The DTC is based on the use of two hysteresis controllers to control the generator electromagnetic torque and the rotor flux respectively. The key issue of the design of the DTC is the strategy used for the selection of a relevant rotor voltage vector to apply to the rotor side converter (RSC) in order to maintain the rotor flux and the developed torque values into their prescribed bands [29,30]. Compared with the oriented vector control, DTC is less sensitive to parameter variations and is characterized by a high dynamic performance [30,3,17,1]. As any control technique has its pros and cons, the classical DTC (C-DTC) has a major inconvenience which is the significant torque and flux undulations due to the hysteresis controllers' nature. As a solution for this problem, several authors have turned to artificial intelligence. Many authors have applied fuzzy logic to the C-DTC for induction machines such as in [20,19,6,26,11]. In fact, the introduction of fuzzy logic has clearly reduced the torque and flux undulations.

In this paper, an improved DTC of a DFIG based wind turbine using fuzzy logic is presented (F-DTC). Fuzzy logic switching vector selection scheme is proposed instead of the hysteresis controllers and the look-up table in order to reduce the high torque and flux undulations. The fuzzy control is robust and its design is relatively simple as it does not demand the knowing of the exact model [2]. The performance of the F-DTC is compared with that of the C-DTC, and the results show that the F-DTC is better in comparison with the C-DTC.

This paper is organized as follows: The modeling of the wind turbine, the speed control and the modeling of the DFIG are presented in Sections 2–4 respectively. The basic concepts of the C-DTC strategy for the DFIG are presented in Section 5. In Section 6, the improved DTC strategy based on fuzzy logic is presented. The simulation results will be discussed in Section 7 and finally the conclusions of this work are given in Section 8.

2. Modeling of the wind turbine

The mechanical power that can be extracted from the wind is a function of the air density ρ, the blade radius R, the wind speed v and the performance coefficient C_p. It can be expressed as follows:

$$P_m = 0.5\rho\pi R^2 v^3 C_p\,(\lambda, \beta) \tag{1}$$

C_p is a function of the wind turbine blade's pitch angle β and the tip speed ratio λ, which is defined by:

$$\lambda = \frac{\Omega_{\text{tur}} R}{v} \tag{2}$$

where Ω_{tur} is the turbine speed.

Cp is given by:

$$C_p\,(\lambda, \beta) = c_1 \left(\frac{c_2}{\lambda_i} - c_3\beta - c_4\right) e^{-\frac{c_5}{\lambda_i}} + c_6\lambda_i \tag{3}$$

$$\frac{1}{\lambda_i} = \frac{1}{\lambda + 0.08\beta} - \frac{0.035}{\beta^3 + 1} \tag{4}$$

C_i: i [1…6] are turbine constants.

The aerodynamic torque is given by:

$$T_{\text{aer}} = \frac{1}{2}.\rho.\pi.R^2.C_p.v^3.\frac{1}{\Omega_{\text{tur}}}. \tag{5}$$

The Gearbox model:

The role of the gearbox is to transform the turbine speed to the generator speed, and the aerodynamic torque to the torque applied on the shaft of the generator according to the following mathematical formulas [7]:

$$T_m = \frac{T_{\text{aer}}}{G} \tag{6}$$

$$\Omega_{\text{mec}} = \Omega_{\text{tur}}.G \tag{7}$$

where Ω_{mec} is the generator speed and T_m is the turbine developed torque.

The dynamic equation of the wind turbine is given by:

$$J\frac{d\Omega_{\text{mec}}}{dt} + f_v.\Omega_{\text{mec}} = T_m - T_{\text{em}} \tag{8}$$

J is the system total inertia, f_v is the friction coefficient and $\mathbf{T_{em}}$ is the generator electromagnetic torque.

3. Speed control: Tip speed ratio based MPPT

The tip speed ratio (TSR) based maximum power point tracking (MPPT) control aims to keep the TSR λ at its optimum value λ_{opt}, which means to determine the turbine optimal speed which achieves the maximum power output.

At this value, $C_p\,(\lambda, \beta)$ is equal to its maximum value. The pitch angle is set to zero due to the assumption of fixed pitch wind turbine [5]. So according to Eq. (2):

$$\Omega_{\text{tur}} = \frac{\lambda v}{R}. \tag{9}$$

Therefore, the referential speed is given by

$$\Omega_{\text{tur\_ref}} = \frac{\lambda_{\text{opt}} v}{R}. \tag{10}$$

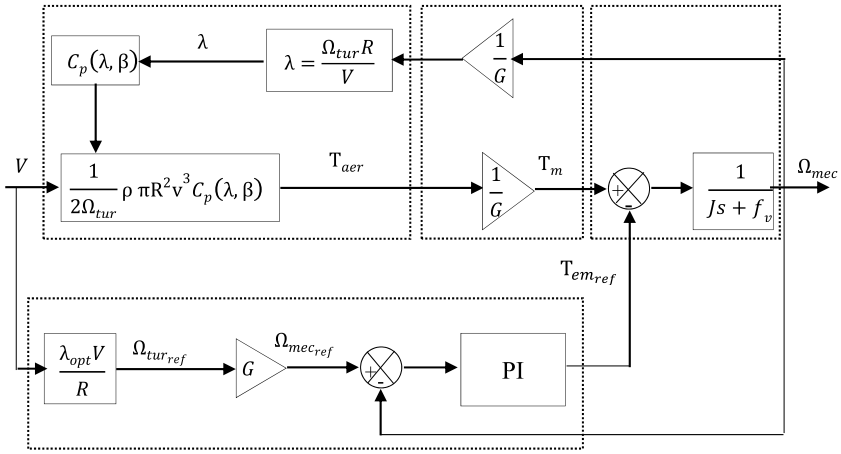

Fig. 1. Diagram block of the TSR based MPPT.

The block diagram of the TSR based MPPT is shown in Fig. 1. Synthesis of the speed proportional and integral (PI) controller (see Fig. 2).

The closed-loop transfer function of the system above is given by:

$$F\,(s) = \frac{\left(K_p + \frac{K_i}{s}\right)\frac{1}{Js+f_v}}{1 + (K_p + \frac{K_i}{s})\frac{1}{Js+f_v}} \tag{11}$$

$$F\,(s) = \frac{K_p s + K_i}{Js^2 + \left(f_v + K_p\right)s + K_i} \tag{12}$$

$F(s)$ is a second order transfer function. It could be written as follows:

$$F\,(s) = \frac{1}{J}\frac{K_p s + K_i}{s^2 + 2\xi\omega_n s + \omega_n^2}. \tag{13}$$

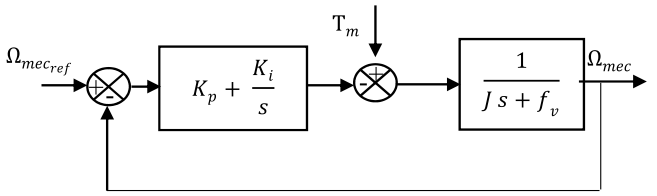

Fig. 2. The PI speed controller.

The expressions of the proportional and the integral gains could be gotten easily using the two previous Eqs. (12) and (13):

$$K_i = J\omega_n^2 \tag{14}$$

$$K_P = 2\zeta J\omega_n - f_v \tag{15}$$

ζ is the damping ratio.
ω_n is the undamped natural frequency.

4. Modeling of the DFIG

The DFIG is a wound rotor induction generator. Its stator windings are connected directly to the three-phase distribution network, while its rotor windings are connected to the bidirectional power converters. The basic structure of a DFIG based wind turbine is shown in Fig. 3.

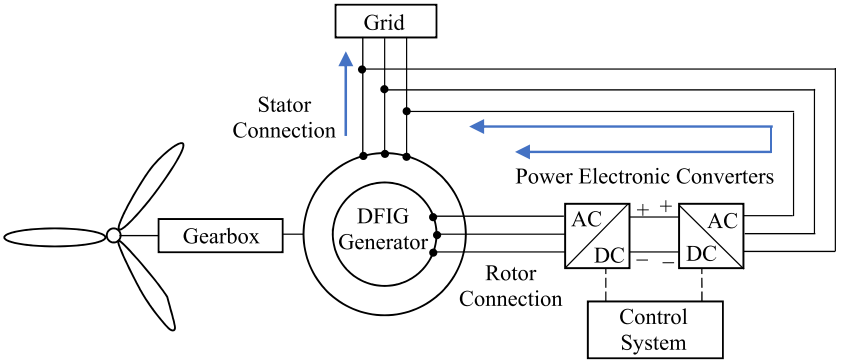

Fig. 3. DFIG-based wind power system.

The application of the Concordia and Park transformations to the three phases of the DFIG makes it possible to write the general model of the DFIG, which is resumed as follows:

$$\begin{aligned}
V_{sd} &= R_s I_{sd} + \frac{d}{dt}\varphi_{sd} - \omega_s \varphi_{sq} \\
V_{sq} &= R_s I_{sq} + \frac{d}{dt}\varphi_{sq} + \omega_s \varphi_{sd} \\
V_{rd} &= R_r I_{rd} + \frac{d}{dt}\varphi_{rd} - \omega_r \varphi_{rq} \\
V_{rq} &= R_r I_{rq} + \frac{d}{dt}\varphi_{rq} + \omega_r \varphi_{rd}
\end{aligned} \tag{16}$$

where:
V_{sd}, V_{sq}, V_{rd} and V_{rq}: The stator and rotor voltages in the d–q frame respectively.
I_{sd}, I_{sq}, I_{rd} and I_{rq}: The stator and rotor currents in the d–q frame respectively.
R_s, R_r: Stator and rotor phase resistances.

The stator and rotor flux d–q components are given as follows:

$$\begin{aligned}\varphi_{sd} &= L_s I_{sd} + M I_{rd}\\ \varphi_{sq} &= L_s I_{sq} + M I_{rq}\\ \varphi_{rd} &= L_r I_{rd} + M I_{sd}\\ \varphi_{rq} &= L_r I_{rq} + M I_{sq}\end{aligned} \tag{17}$$

M: The mutual inductance.
L_s, L_r: Stator and rotor inductances.

The torque generated by the DFIG [1]:

$$T_{\text{em}} = \frac{3}{2}\frac{pM}{L_s}\left(\varphi_{s\alpha} I_{r\beta} - \varphi_{s\beta} I_{r\alpha}\right) \tag{18}$$

p: Poles number of the machine.

5. Classical direct torque control

The C-DTC method is based on the selection of an adequate rotor voltage vector to apply to the RSC using the torque and rotor flux information in order to control the generator electromagnetic torque and rotor flux. The three phase RSC has three control switches S_a, S_b and S_c. Their combinations can generate eight switching states of the rotor voltage vector V_r, six active vectors and two zero ones [8]. These vectors can divide the plan into six sectors. The rotor flux vector might be located in one of these sectors.

The C-DTC technique block diagram is shown in Fig. 4.

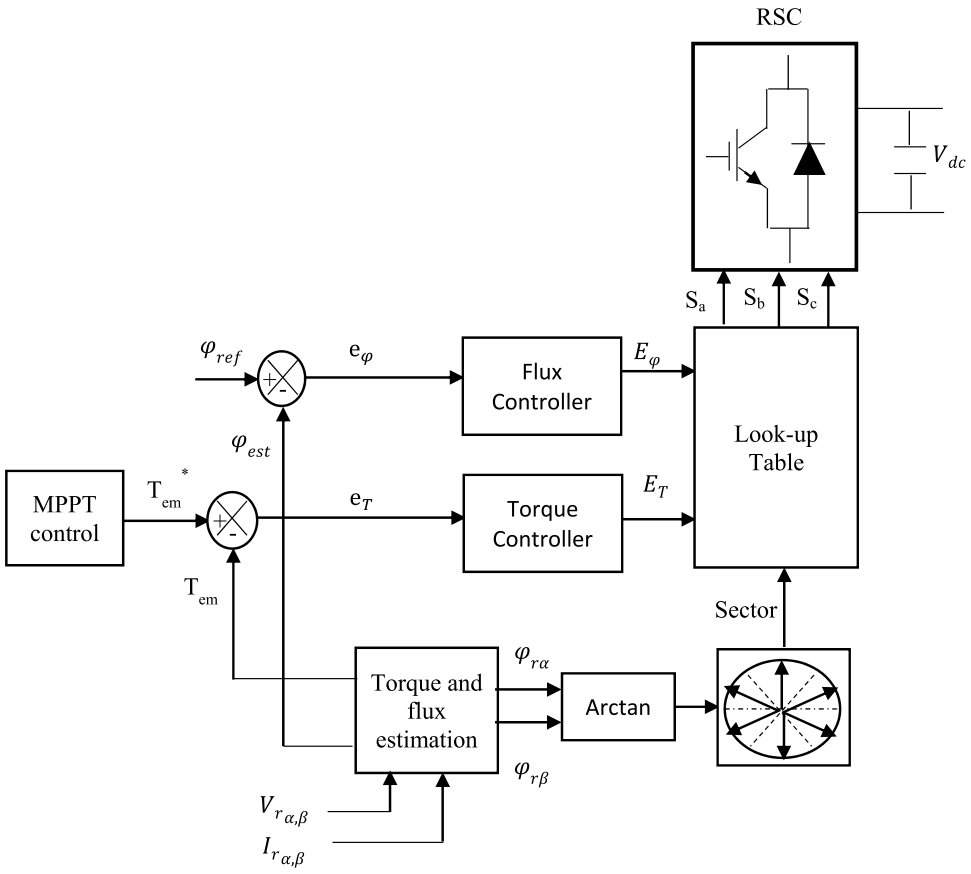

Fig. 4. The classical DTC of the DFIG.

The estimated rotor flux magnitude and the estimated electromagnetic torque are compared with the referential rotor flux and the referential electromagnetic torque gotten from the MPPT block respectively, and the errors are used as inputs of the hysteresis controllers (Figs. 5 and 6) in order to control the torque and rotor flux, and to maintain the rotor flux vector extremity in a circular trajectory as it is shown in Fig. 7 [19]. The output of both hysteresis controllers is a Boolean variable specifying if the flux/torque should be increased or decreased [14] to allow the application of the suitable rotor voltage vector to the system [21].

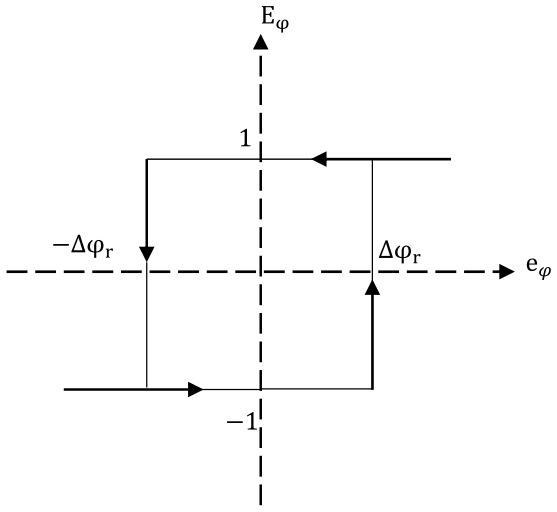

Fig. 5. The rotor flux hysteresis controller.

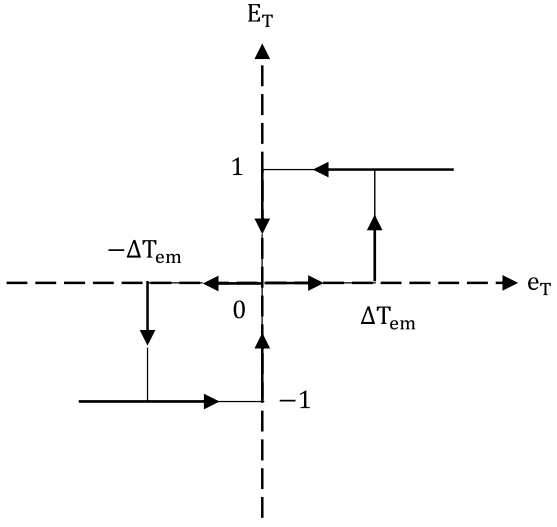

Fig. 6. The electromagnetic torque hysteresis controller.

$\Delta\varphi_r$, ΔT_{em}: The rotor flux and electromagnetic torque hysteresis controllers bandwidth respectively.

Rotor flux control:

The rotor flux magnitude is determined as follows [14]:

$$\varphi_r = \sqrt{\varphi_{r\alpha}^2 + \varphi_{r\beta}^2} \tag{19}$$

$\varphi_{r\alpha}$ and $\varphi_{r\beta}$ are the DFIG rotor flux components in the α, β frame respectively, they are usually estimated by integrating the rotor voltage:

$$\varphi_{r_{\alpha,\beta}} = \int_0^t \left(V_{r_{\alpha,\beta}} - R_r I_{r_{\alpha,\beta}}\right) dt. \tag{20}$$

The voltage drop due to the rotor resistance ($R_r I_{r_{\alpha,\beta}}$) can be neglected compared to Vr, so [1]:

$$\overline{\varphi}_{r_{\alpha,\beta}} = \overline{\varphi}_{r_{\alpha,\beta_0}} + \int_0^{\Delta t} \overline{V}_{r_{\alpha,\beta}} dt \tag{21}$$

where:

$\overline{\varphi}_{r_{\alpha,\beta_0}}$: is the rotor vector flux at $t = 0$ s.

Δt: the sampling time.

$$\overline{\varphi}_{r_{\alpha,\beta}} = \overline{\varphi}_{r_{\alpha,\beta_0}} + \overline{V}_{r_{\alpha,\beta}} \Delta t. \tag{22}$$

During a periodic control interval [0 Δt], the rotor voltage vector is considered constant, therefore, Eq. (22) could be written as follows:

$$\overline{\varphi}_r(k+1) \approx \overline{\varphi}_r(k) + \overline{V}_r \Delta t \tag{23}$$

$$\text{which is equivalent to :} \quad \Delta\overline{\varphi}_r = \overline{V}_r \Delta t \tag{24}$$

where: $\overline{\varphi}_r(k)$: is the rotor flux vector at the current sampling rate.

$\overline{\varphi}_r\ (k+1)$: is the rotor flux vector at the next sampling rate.

$\Delta\overline{\varphi}_r$: the variation of the rotor flux vector.

Eq. (24) implies that for a constant sampling period Δt, the rotor flux voltage vertex moves according to the direction given by the voltage vector V_r. Therefore, the rotor flux is controlled by V_r.

Electromagnetic torque control:

The electromagnetic torque generated by DFIG could be estimated using Eq. (18) which could be written as follows [1]:

$$T_{\text{em}} = \frac{3}{2} p \frac{M}{L_r L_s - M^2} |\varphi_s| \, |\varphi_r| \, sin\theta \tag{25}$$

θ: The phase angle difference between the rotor flux and the stator flux.

$$\theta = arctan\left(\frac{\varphi_{r\beta}}{\varphi_{r\alpha}}\right). \tag{26}$$

As the DFIG stator winding is connected to the grid which is assumed stable, the stator flux magnitude $|\varphi_s|$could be regarded as constant when the voltage drop on the stator winding resistance R_s is neglected [17]. Therefore, according to Eq. (25), the torque is controlled by the rotor flux magnitude $|\varphi_r|$ and the angle θ.

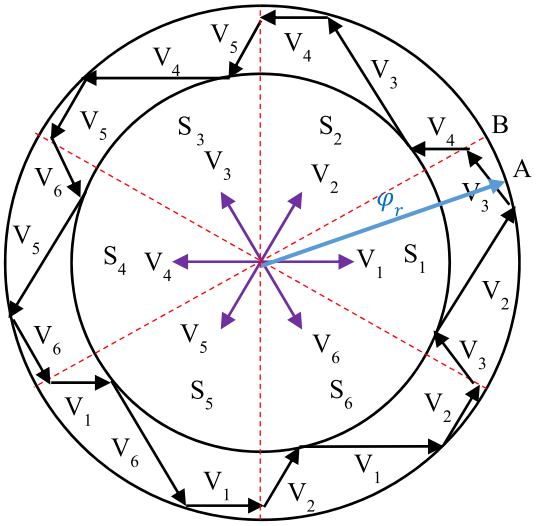

Fig. 7. The representation of the rotor flux vector trajectory according to different voltage vectors.

The location of the rotor flux vector in the six sectors is determined according to the phase angle difference θ. Therefore, to increase the electromagnetic torque, the rotor flux vector summit should be rotated as much as possible counterclockwise. If the torque should be decreased, the flux vector should be rotated clockwise.

For example, let us suppose that the flux vector is in the first sector on its upper limit (A). Furthermore, we want to increase the torque and we want to keep the flux at the upper limit, then the vector V3 is applied to move the flux vector vertex to B. If we want to increase the torque again and to decrease the rotor flux, in that case the vector V4 is applied, and flux vector vertex is moved to C... etc. Then the selection is carried out according to the switching table (Table 1).

Table 1
The C-DTC switching table for the optimal rotor voltage vector selection.

Sector		1	2	3	4	5	6
$E_F = 1$	$E_T = 1$	V2	V3	V4	V5	V6	V1
	$E_T = 0$	V7	V0	V7	V0	V7	V0
	$E_T = -1$	V6	V1	V2	V3	V4	V5
$E_F = -1$	$E_T = 1$	V3	V4	V5	V6	V1	V2
	$E_T = 0$	V0	V7	V0	V7	V0	V7
	$E_T = -1$	V5	V6	V1	V2	V3	V4

6. Fuzzy direct torque control

The proposed F-DTC control aims to improve the C-DTC performances. It is based on the use of a fuzzy inference system instead of the hysteresis band controllers and the look-up table.

For the proposed system, the inputs are: the rotor flux error, the electromagnetic torque error and the sector identification angle θ. The converter switches S_a, S_b and S_c are used as outputs (see Fig. 8).

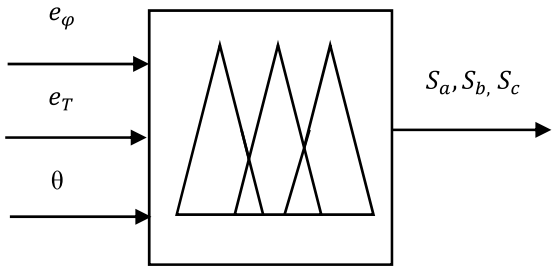

Fig. 8. The proposed fuzzy inference system.

The fuzzy controller observes the errors signals and the sector identification angle, and correspondingly updates the output voltage vector so that the electromagnetic torque and the rotor flux match their references.

$$e_\varphi = \varphi_r^* - \varphi_r \tag{27}$$

$$e_T = T_{\text{em}}^* - T_{\text{em}}. \tag{28}$$

To design a fuzzy inference system, the following steps must be performed:

- Fuzzification: It consists of taking the inputs and converting them to a fuzzy set using linguistic terms and membership functions (MFs).
- Fuzzy rules: This step consists of the development of a suitable rule set which is similar to the human brain in the decisions and choices making process [24]. Once the input, output variables and MFs are defined, the rule-base composed of expert IF <antecedents> THEN <conclusions> rules has to be designed [22], [28].
- Defuzzification: It consists of the conversion of the aggregated fuzzy set to a precise real value.

6.1. Fuzzification

Simple triangular MFs are used for the inputs, while singleton MFs are used for the outputs, they are illustrated in Figs. 9–12. The linguistic variables used for the MFs are:

- For the flux error: Negative (N) and Positive (P).
- For the torque error: Negative, positive and Zero (Z).
- For the sector angle determination: $\theta_1$to θ_7.
- For the converter's switches $S_i(S_a, S_b$ and $S_c)$: 0 and 1.

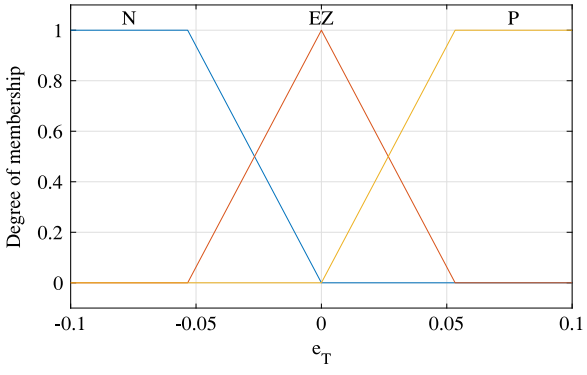

Fig. 9. The torque error membership functions.

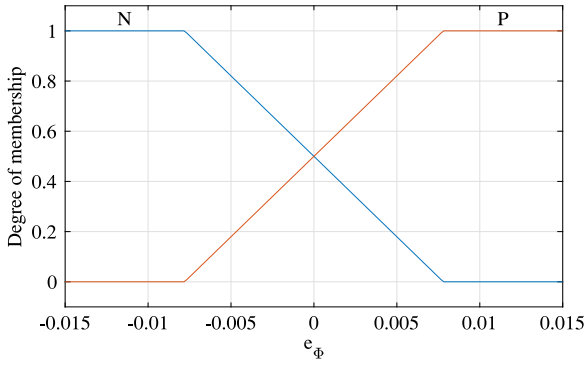

Fig. 10. The rotor flux error membership functions.

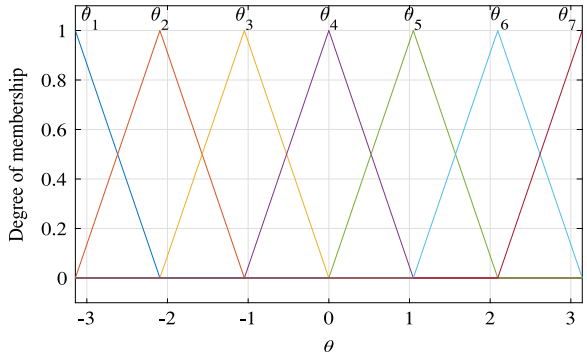

Fig. 11. The sector identification angle membership functions.

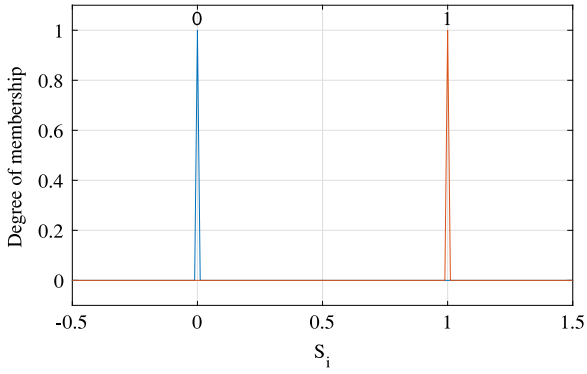

Fig. 12. The output S_i membership functions.

6.2. *Fuzzy rules*

After the inputs are fuzzified, appropriate rule-base should be developed using the inputs and the outputs. Which can be described as [10]:

IF(e_φ is $A_{p,n}$) AND (e_T is $B_{p,n,z}$) AND (θ is $\theta_{1,7}$) THEN (S_a is $D_{0,1}$) AND (S_b is $D_{0,1}$) AND (S_c is $D_{0,1}$).

where $A_{p,n}$, $B_{p,n,z}$, $\theta_{1,7}$ and $D_{0,1}$ are the inputs and outputs fuzzy sets.

The inputs of the fuzzy inference system have two, three and seven fuzzy sets respectively, which gives a set of forty-two rules ($2 * 3 * 7$). These rules could be represented by the following inference matrix (see Table 2).

Table 2
The fuzzy rules.

e_φ	e_T	θ_1	θ_2	θ_3	θ_4	θ_5	θ_6	θ_7
N	N	110	010	011	001	101	001	110
	Z	111	000	111	000	111	000	111
	P	101	100	110	010	011	010	101
P	N	010	011	001	101	100	101	010
	Z	000	111	000	111	000	111	000
	P	001	101	100	110	010	110	001

6.3. Defuzzification

To get the output of the fuzzy inference system, which means to determine the switches' state if it should be 0 or 1 (opened or closed respectively). The Mean of Maximum (MOM) defuzzification method is used. This method calculates the most plausible result by selecting the highest value of the most valid output linguistic term.

Since the entire shape of the output MFs is a singleton shape (for $S_i = 0$ and 1), in all the cases the outputs that will give these highest values will be only 0 or 1 for each output.

7. Simulations and results analysis

The simulation was carried out for the same conditions for both the C-DTC and F-DTC, and has been performed in MATLAB Sim Power Systems toolbox. The simulation parameters are given in Table 3 [15]:

Table 3
The DFIG and wind turbine parameters.

R_s	0.455 Ω
R_r	0.62 Ω
L_s	0.084 H
L_r	0.081 H
M	0.078 H
J	0.3125 kg m^2
F	6.73e^{-3} N m s rad
c_1	0.5176
c_2	116
c_3	0.4
c_4	5
c_5	21
c_6	0.0068

The wind speed is subjected to a varied wind speed, varying from 10 m/s to 11 m/s (see Fig. 13). The referential rotor flux magnitude is set to 0.98 Wb, and the referential torque is obtained from the MPPT control.

The rotor flux magnitude response for both strategies is shown in Figs. 14 and 15. As we can see in Fig. 16, which is a zoom of the previous figures, the classical DTC strategy represents high ripples and it is clearly seen that the F-DTC provides a better response and less ripples.

Fig. 17 shows the response of the mechanical speed for both techniques. It is clearly seen that the mechanical speed tracks perfectly its reference for both strategies, which proves the efficiency of the MPPT control. As the wind speed changes, the rotor speed matches its reference gotten from the MPPT control to ensure the maximum wind power.

Figs. 18 and 19 show the electromagnetic torque response for the classical technique and the improved one. For both control techniques, the estimated torque tracks closely its reference. Moreover, the torque ripples are minimized with the improved DTC technique as it can be seen in Fig. 20.

As can be clearly seen in Figs. 21 and 22, the rotor flux trajectory is kept circular for both control schemes, but it presents relatively large ripples in the C-DTC.

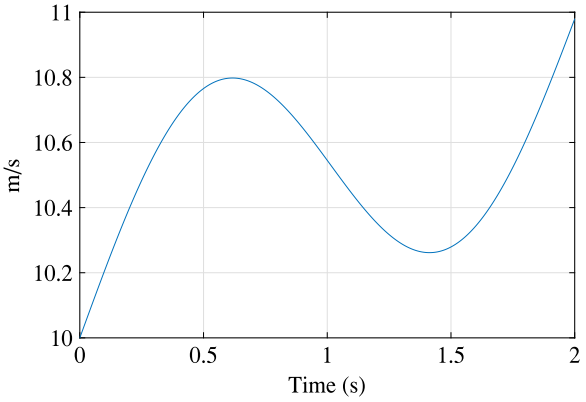

Fig. 13. The wind speed profile.

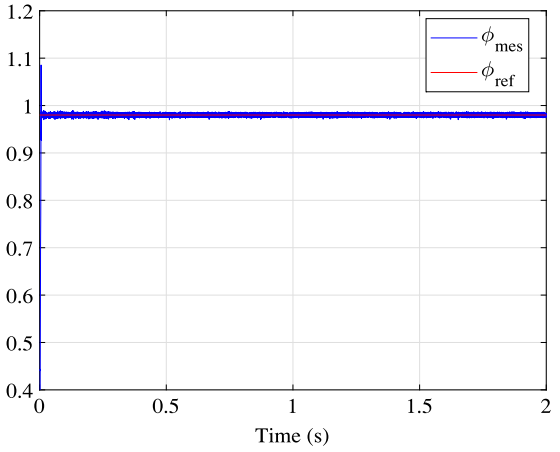

Fig. 14. The rotor flux magnitude for C-DTC (Wb).

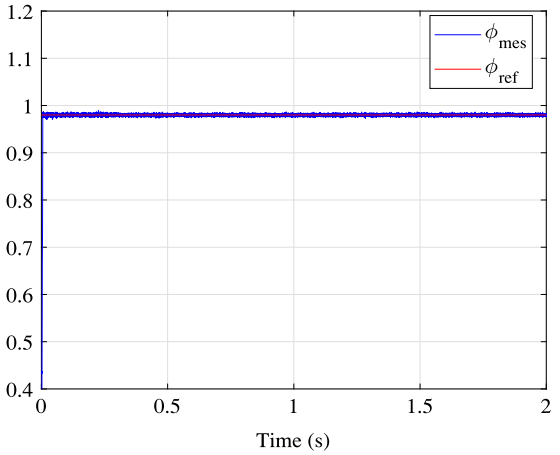

Fig. 15. The rotor flux amplitude for F-DTC (Wb).

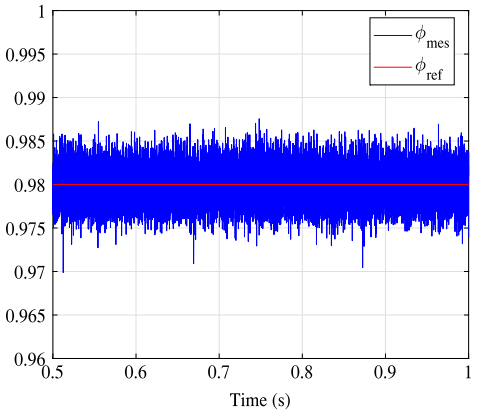

(a) C-DTC.

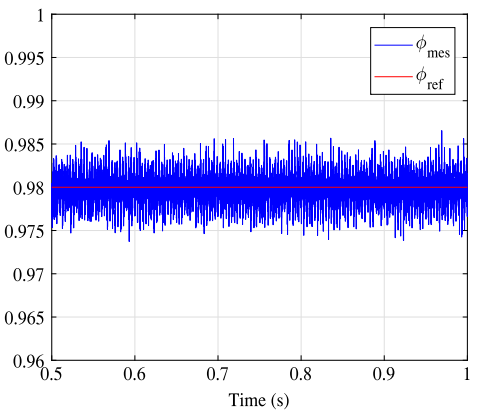

(b) F-DTC.

Fig. 16. Zoom on the rotor flux amplitude (Wb).

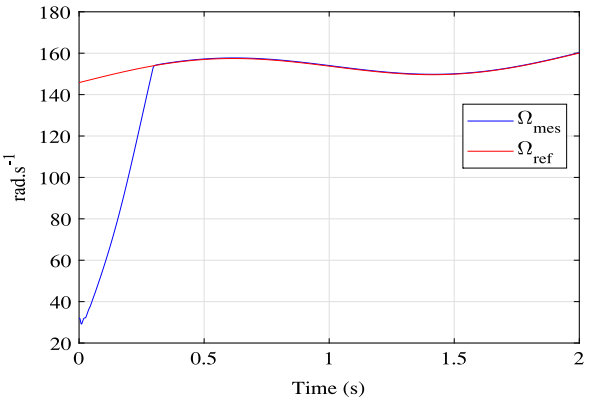

Fig. 17. The turbine mechanical speed for both strategies.

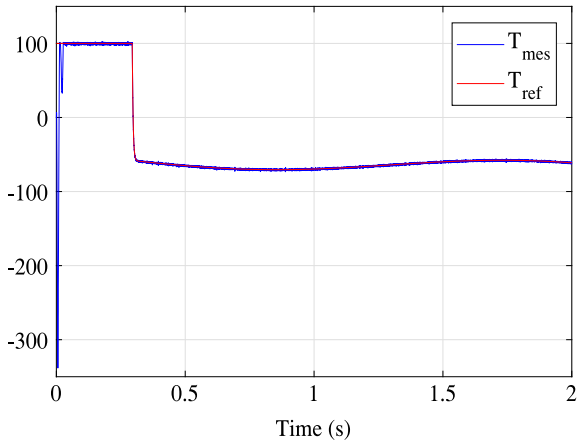

Fig. 18. The electromagnetic torque for C-DTC (N m).

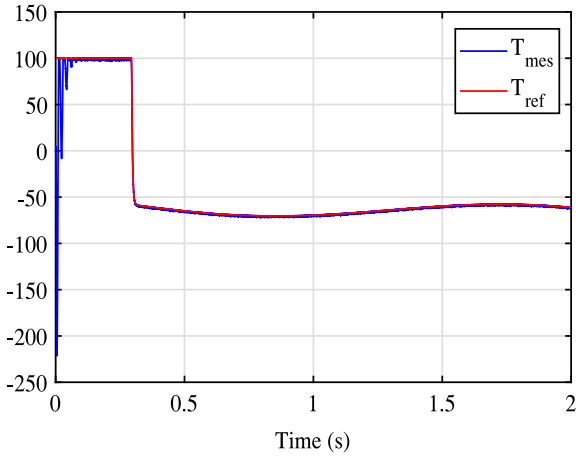

Fig. 19. The electromagnetic torque for F-DTC (N m).

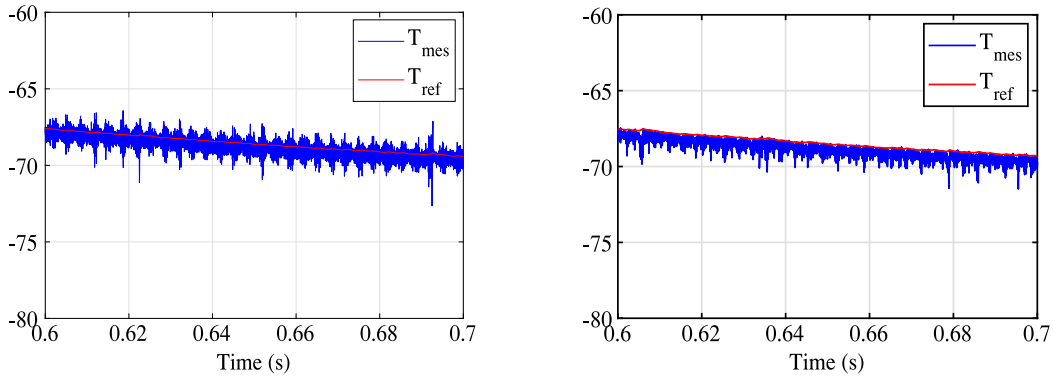

(a) C-DTC. (b) F-DTC.

Fig. 20. Zoom on the electromagnetic torque amplitude (N m).

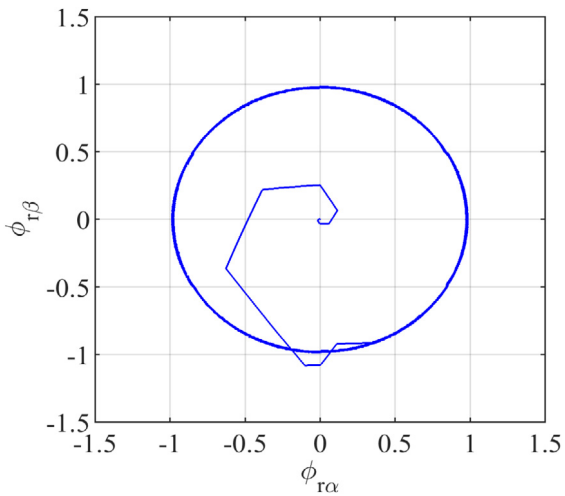

Fig. 21. Rotor flux trajectory (C-DTC).

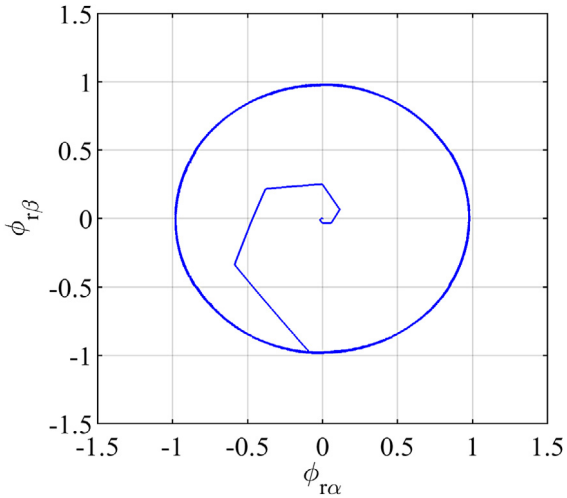

Fig. 22. Rotor flux trajectory (F-DTC).

In order to compare the performance of the proposed control technique with the classical one, the root mean square error (RMSE) criterion has been used to measure the divergence of the measured values with the referential ones. The lower the RMSE is, the better the fit of the model. The RMSE is calculated using the following Eq. (29):

$$RMSE = \sqrt{\frac{\sum_{i=1}^{n} \left(y_{\mathrm{ref}_i} - y_{\mathrm{mes}_i}\right)^2}{n}} \tag{29}$$

y_{ref_i}: The referential values.
y_{mes_i}: The measured values.
n: Sample size.

For the rotor flux magnitude, the RMSE of the C-DTC is 0.0021 Wb, while for the F-DTC is 0.0012 Wb, which means a reduction of 43%. For the electromagnetic torque, the RMSE of the C-DTC is 0.5282 N m, while for the F-DTC is 0.4924 N m, which means a reduction of 7%.

In order to better illustrate the impact of the C-DTC on the quality of the signal provided by the DFIG, a FFT (Fast Fourier Transform) analysis of the stator and rotor currents waveforms of phase (a) was carried out for 3 cycles of operation starting at 0.4 s and for a harmonic order of 30. The frequency spectrum is illustrated in Figs. 23 and 24. The analysis showed that the F-DTC provides a lower total harmonic distortion (THD) in comparison with the C-DTC. For the rotor current and stator current, with the C-DTC strategy, the THD rate is 6.60% and 7.69% respectively. While in the case of the F-DTC, the THD rate is 2.01% and 2.03% respectively.

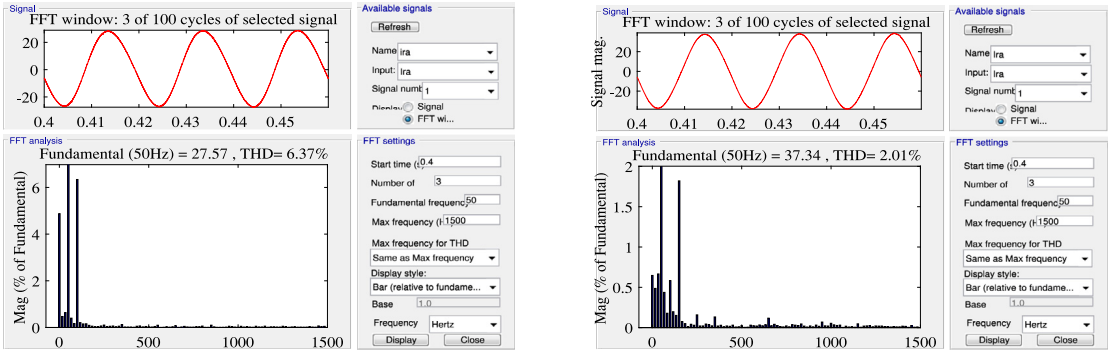

(a) C-DTC. (b) F-DTC.

Fig. 23. The FFT analysis of phase (a) rotor current.

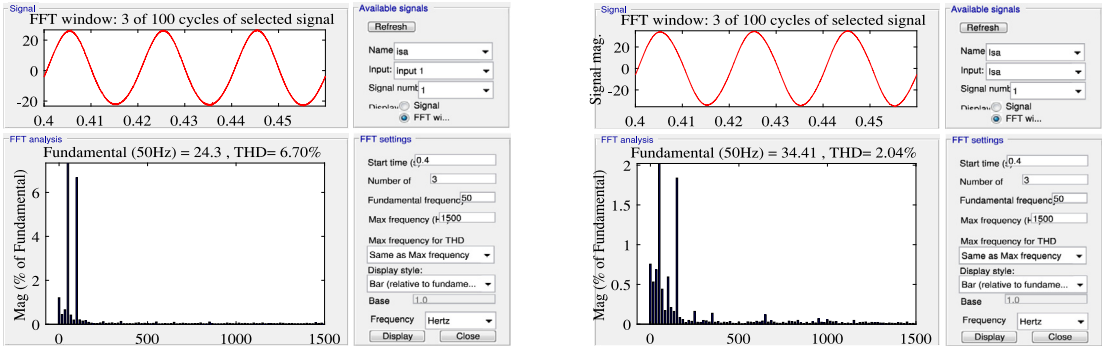

(a) C-DTC. (b) F-DTC.

Fig. 24. The FFT analysis of phase (a) stator current.

8. Conclusions

An improved direct torque control technique for a DFIG based wind turbine has been investigated in this paper. The proposed control technique is based on improving the classical technique by replacing the hysteresis controllers and the look-up table by a fuzzy inference system. The simulation has been performed in Matlab/Simulink to compare the proposed system with the classical one. According to the results obtained, the main objectives were achieved. It becomes clear that the proposed F-DTC strategy gives good performance in comparison with the C-DTC, such as the perfect tracking of the references which was proved by the RMSE criterion and the reduction of torque and flux ripples. In addition, the FFT analysis of the rotor and stator currents showed a lower total harmonic distortion, which means an improvement of the quality of current signals. Moreover, the hysteresis controllers and the look-up table used in the classical method are removed.

Thus, a future study can be extended to study the design and real implementation of the proposed control technique on a FPGA.

References

[1] G. Abad, J. Lopez, M.A. Rodriguez, L. Marroyo, G. Iwanski, Doubly Fed Induction Machine, John Wiley & Sons, Inc., Hoboken, New Jersey, 2011.

[2] S.C. Abou, T.-M. Dao, Integrated mining fuzzy association rules for mineral processing state identification, in: M. Ao, Sio-Iong Rieger, Burghard B. Amouzegar (Eds.), Machine Learning and Systems Engineering, Springer, 2010, pp. 311–325.

[3] A. Al-Quteimat, A. Roccaforte, U. Schäfer, Control for doubly fed induction generator with 12 sector methodology, in: 5th International Conference on Renewable Energy Research and Applications, Vol. 5, 2016.

[4] Y. Amirat, M. Benbouzid, E. Al-ahmar, B. Bensaker, A brief status on condition monitoring and fault diagnosis in wind energy conversion systems, Renew. Sustain. Energy Rev. Elsevier 3 (9) (2009) 2629–2636.
[5] C. Balasundar, S. Sudharshanan, R. Elakkiyavendan, Design of an optimal tip speed ratio control MPPT algorithm for standalone WECS, Int. J. Res. Appl. Sci. Eng. Technol. 3 (V) (2015).
[6] Y. Bendaha, Fuzzy direct torque control of induction motor with sensorless speed control using parameters machine estimation, in: 3rd International Conference on Control, Engineering & Information Technology (CEIT), 2015.
[7] K. Berkoune, E. Ben Sedrine, L. Vido, S. Le Ballois, Robust control of hybrid excitation synchronous generator for wind applications, Math. Comput. Simulation 131 (2015) 55–75.
[8] R. Cárdenas, R. Peña, S. Alepuz, G. Asher, Overview of control systems for the operation of DFIGs in wind energy applications, IEEE Trans. Ind. Electron. 60 (7) (2013) 2776–2798.
[9] M. El Achkar, R. Mbayed, G. Salloum, N. Patin, S. Le Ballois, E. Monmasson, Power operating domain of a cascaded doubly fed induction machine Power operating domain of a cascaded doubly fed induction machine, Math. Comput. Simulation (2015).
[10] J. Espinosa, J. Vandewalle, V. Werts, Fuzzy Logic, Identification and Predective Control (Advances in Industrial Control), Springer, 2004.
[11] Y. Gao, J. Wang, X. Qiu, The improvement of DTC system performance on fuzzy control, Procedia Environ. Sci. 10 (2011) 589–594.
[12] B.D. Gidwani, Wind energy conversion system using back to back power electronic interface with DFIG, in: Recent Advances in Energy, Environment and Financial Planning, 2014, no. 3, pp. 330–334.
[13] GWEC's Global Wind Report - Annual Market Update, the Global Wind Energy Council, 2017. [Online]. Available: http://www.gwec.net.
[14] I. Hamzaoui, F. Bouchafaa, A. Talha, S.G. Malla, Advanced control for wind energy conversion systems with flywheel storage dedicated to improving the quality of energy, Int. J. Hydrog. Energy 41 (45) (2016) 20832–20846.
[15] K. Kerrouche, A. Mezouar, K. Belgacem, Decoupled control of doubly fed induction generator by vector control for wind energy conversion system, Energy Procedia 42 (2013) 239–248.
[16] R. Kot, M. Rolak, M. Malinowski, Comparison of maximum peak power tracking algorithms for a small wind turbine, Math. Comput. Simulation (2013).
[17] Y. Li, et al., An improved DTC controller for DFIG-based wind generation system, in: 2016 IEEE 8th International Power Electronics and Motion Control Conference, 2016, pp. 6–9.
[18] M. Machmoum, A. Hatoum, T. Bouaouiche, Flicker mitigation in a doubly fed induction generator wind turbine system, Math. Comput. Simulation 81 (2) (2010) 433–445.
[19] S.G. Malla, A Review on direct torque control (DTC) of induction motor : with applications of fuzzy, in: International Conference on Electrical, Electronics, and Optimization Techniques (ICEEOT), 2016, pp. 4557–4567.
[20] J. Mohana Rao Malla, M. Kumar Sahu, P.K. Subudhi, DTC-SVM of induction motor by applying two fuzzy logic controllers, in: International Conference on Electrical, Electronics, and Optimization Techniques (ICEEOT), 2016, Vol. 2, no. 11, pp. 1956–1969.
[21] E. Monmasson, J.P. Louis, Presentation of a control law for IM drive based on the dynamic reconfiguration of a DTC algorithm and a SVM-DTC algorithm, Math. Comput. Simulation 63 (2003) 321–333.
[22] R.R. Patel, A.N. Shewale, Intelligent sun tracking system using FLC implemented on FPGA, Int. J. Adv. Found. Res. Comput. 2 (10) (2015) 260–263.
[23] Ren21, Renewables 2017 global status report 2017, 2017.
[24] P. Sevastianov, L. Dymova, Synthesis of fuzzy logic and Dempster–Shafer theory for the simulation of the decision-making process in stock trading systems, Math. Comput. Simulation 80 (2009) 506–521.
[25] S. Sharma, Simulation and analysis of DFIG system with wind turbine implementing fuzzy logic controller, in: 1st International Conference on Non Conventional Energy, 2014, no. Iconce, pp. 154–159.
[26] G. Sung, W.-S. Lin, S.-K. Peng, Reduction of torque and flux variations using fuzzy direct torque control system in motor drive, in: 2013 IEEE International Conference on Systems, Man, and Cybernetics, 2013.
[27] P. Tchakoua, R. Wamkeue, M. Ouhrouche, F. Slaoui-hasnaoui, T.A. Tameghe, G. Ekemb, Wind turbine condition monitoring: state-of-the-art review, new trends, and future challenges, Energies (2014) 2595–2630.
[28] R. Velmurugan, R. Jeyabharath, Fuzzy logic based harmonic minimization in cascaded multilevel inverter, Int. J. Eng. Res. Electr. Electron. Eng. 2 (4) (2016) 40–44.
[29] L. Youb, A. Craciunescu, Direct torque control of induction motors with fuzzy minimization torque ripple, in: Proceedings of the World Congress on Engineering and Computer Science, Vol. II, 2009.
[30] Y. Zhang, Z. Li, T. Wang, W. Xu, J. Zhu, Evaluation of a class of improved DTC method applied in DFIG for wind energy applications, in: 2011 International Conference on Electrical Machines and Systems, 2011, pp. 1–6.